Synthesis and Crystallization of N-rich Triazole Compounds

Emmanuele Parisi * and Roberto Centore

Posted Date: 2 November 2023

doi: 10.20944/preprints202311.0186.v1

Keywords: Crystal Engineering; N-Rich compounds; triazole system; HEDM

Article

Synthesis and Crystallization of N-Rich Triazole Compounds

Emmanuele Parisi [1,*] and Roberto Centore [2]

[1] Department of Science and Applied Technology, Politecnico di Torino, Corso Duca degli Abruzzi 24, I-10129, Torino

[2] Department of Chemical Sciences, Università degli Studi di Napoli Federico II, Via Cinthia, I- 80126, Napoli; roberto.centore@unina.it

* Correspondence: emmanuele.parisi@polito.it

Abstract: Among N-rich heterocycle backbone compounds the triazoles building block received a lot interest in several different academic and industrial study and application. This articles outlines the process of synthesizing three different 1,2,4-triazole-based systems, commencing with 1,3-diaminoguanidine hydrochloride monohydrate as starting material. The structure of the obtained crystals was established by NMR spectroscopy and single-crystal X-Ray diffraction analysis. Hirshfeld surface analysis was employed to explore the intermolecular interactions that are responsible for crystal packing quantitatively. The synthesized compounds, with their elevated nitrogen content, serve as potentially components for High-Energy-Density material science applications.

Keywords: crystal engineering; N-rich compounds; triazole system; HEDM; Hirshfeld Surface

1. Introduction

Heterocyclic compounds, and nitrogen-rich hetero compounds, are widespread in nature and play numerous roles in the physiology of living organisms. They are present in vitamins, amino acids (proline, histidine and tryptophan), in biologically active compounds [1], such as chlorophyll and heme (structurally consisting of derivatives of porphyrins rings), in medicines (including anti-inflammatory, antimalarial, antimicrobial, antiviral, antidiabetic), synthetic agrochemicals (herbicides and insecticides) and natural bioactive substances such as alkaloids, caffeine, etc. Undoubtedly, it is crucial to highlight their significance as fundamental biological molecules that constitute DNA and RNA. Moreover, the growing utilization of N-rich aromatics as foundational components for crafting conjugated active molecules with applications across a range of advanced materials fields, including semiconducting polymers [2], organic field-effect transistors [3], fluorescent sensors [4,5], organic solar cells [6,7] and high-energy-density compounds [8–11] merits attention. An intriguing and peculiar feature of many heterocyclic systems with high nitrogen content is tautomerism [12–17]. Tautomerization reactions typically entail the shifting of a lone hydrogen atom, which is why they are commonly linked to molecules that have acidic functional groups. This holds particular relevance in the context of crystal engineering because the precise location of a hydrogen atom within the molecule significantly influences its potential to establish hydrogen bonds. Consequently, this has implications for synthon formation and, consequently, the overall packing arrangement. Quasi-degenerate tautomers are a fascinating occurrence. In this case, in fact, the equilibrium mixture contains appreciable amounts of all tautomers. Crystallization represents one of the limited methods available for the separation of distinct tautomers, primarily because it is unlikely to detect various tautomeric forms within the same crystal structure [18]. For quasi-degenerate tautomeric systems, co-crystallization of two tautomers in the same lattice is a possibility, but still a rare phenomenon; another possibility is the precipitation of different crystal forms, each with its own tautomer. These two occurrences account for no more than 0.5 % of molecules in the Cambridge

Preprints (www.preprints.org) | NOT PEER-REVIEWED | Posted: 2 November 2023 doi:10.20944/preprints202311.0186.v1

Structural Database, which is another reason why quasi-degenerate tautomeric systems are particularly interesting. In recent years, our focus has been directed toward the synthesis and examination of benzimidazole [19–21] and N-rich triazole derivatives [5,10,15,16,22–24] in order to investigate their chemico-physical properties and tautomerism. Here we report the synthesis and crystallization of five novel N-rich triazole systems with Nitrogen content between 55 and 70% w/w potentially interesting in HEDMs application (Scheme 1). In this context, energetic heterocyclic compounds with high nitrogen content have emerged as a viable alternative to traditional HEDMs because of their higher stability and environmental friendliness. [25] Energetic materials typically release energy through oxidation processes when they decompose, and nitrogen-rich heterocyclic compounds are no exception. These com-pounds contain nitrogen atoms that are often involved in single or double bonds, and when the molecule decomposes, it generates N_2. The production of nitrogen gas as the primary byproduct makes the entire process environmentally friendly. This effect becomes more pronounced as the nitrogen content of the molecule increases, as it leads to reduced quantities of other byproducts. Furthermore, an increased nitrogen-to-carbon and hydrogen ratio enhances density, which is also desirable. Another valuable aspect of nitrogen-rich heterocyclic compounds is the presence of acidic or basic functional groups, often in the form of basic nitrogen atoms or acidic N-H groups. These features can be harnessed to form salts where the nitro-gen-rich heterocycle serves as a cation or anion. Such salts typically exhibit high stability and can possess diverse properties depending on the choice of counterion.

Triaz1

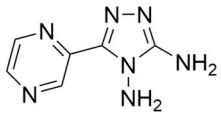

5-(pyrazin-2-yl)-4*H*-1,2,4-triazole-3,4-diamine

Triaz2

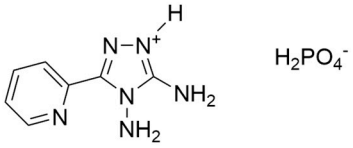

4,5-diamino-3-(pyridin-2-yl)-4*H*-1,2,4-triazol-1-ium dihydrogenphosphate

Triaz3

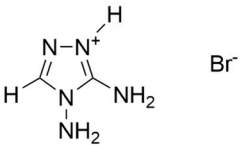

4,5-diamino-4*H*-1,2,4-triazol-1-ium bromide

Triaz4

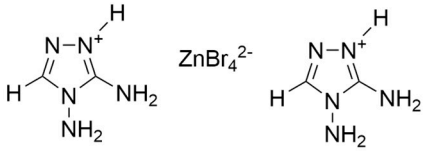

bis(4,5-diamino-4*H*-1,2,4-triazol-1-ium) zinc(II) tetrabromide

Triaz5

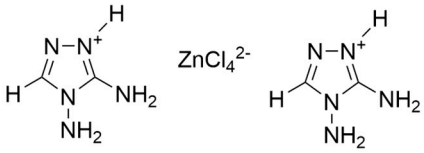

bis(4,5-diamino-4*H*-1,2,4-triazol-1-ium) zinc(II) tetrachloride

Scheme 1. The five novel diaminotriazole compounds described in this paper.

2. Experimental

2.1. Materials and Methods

Caution! The title complexes possess the potential to function as high-energy materials that may detonate under specific circumstances. Despite our incident-free experience in the preparation and handling of these complexes, it is crucial to recognize their energetic nature. Therefore, it is advisable to implement proper safety precautions, including wearing protective gear such as leather coats,

 doi:10.20944/preprints202311.0186.v1

safety glasses, face shields, and ear plugs, particularly when working with these compounds on a larger scale. Starting materials were purchased from Sigma Aldrich, AlfaAesar and Fluorochem and used without further purification. All solvents were use with analytical grade. **3,4-diamino-1,24-triazolium chloride (DATr-HCl)** was synthesized according to a literature procedure [26]. **Triaz1** and **Triaz2** were synthetized by following a slightly modified version of a literature procedure [27]. The synthetic procedures are reported in detail in the following. Compounds' identity was confirmed by Bruker Avance 400 MHz, Varian Inova 500 MHz NMR spectrometers. Temperature controlled optical microscopy were performed with a Zeiss Axioskop polarizing microscope equipped with a Mettler FP90 heating stage for the measurement of the melting point of the synthetized compounds. All data for crystal structure determinations were measured on a Bruker-Nonius KappaCCD diffractometer equipped with Oxford Cryostream 700 apparatus, using graphite monochromated MoKα radiation (0.71073 Å). Data were collected at room temperature and at -100 °C. Reduction of data and semiempirical absorption correction were done using SADABS program [28]. The structures were solved by direct methods (SIR97 pro-gram) [29] and refined by the full-matrix least-squares meth-od on F^2 using SHELXL-2016 program [30] with the aid of the program WinGX. [31] H atoms bonded to C were generated stereochemically and refined by the riding model; those bonded to O and N were found in difference Fourier maps and their coordinates were refined. To all H atoms, U_{iso} equal to 1.2 times U_{eq} of the carrier atom was given. The analysis of the crystal packing was performed using the program Mercury [32]. Hirshfeld surface and potential energy surface were calculated using the program CrystalExplorer21.5 [33]. Crystallographic data for each X-ray single crystal were extracted from their crystallogaprahic information files (.cif) and then imported into Crystal Explorer to produce the Hirshfeld surfaces. Th setting used were as follows: property: none; resolution: high (standard). For fingerprint generation (di vs. de plot) we employed the following parameters: range-standard; filter- by elements; fingerprint-filter options are both inside–outside elements, including reciprocal contacts. Interactions in crystal structures with normalized contact distances shorter than the sum of the respective van der Waals radii of the atoms are depicted as red spots, while those with longer contacts exhibiting positive d_{norm} value are represented in blue.

*2.2. Syntheses and Crystallization of Compounds **Triaz1-Triaz5***

Heterocycles such as triazoles and tetrazole are directly obtained from aminoguanidine [34]. Hereby, diaminoguanidine hydrochloride salt was used for the synthesis of 1,2,4-triazole compounds.

Triaz1: Commercial 2-pyrazinic acid (5.00 g, 40.3 mmol) and diaminoguanidine monohydrochloride (6.58 g, 52.4 mmol, 30% excess by mol) were finely ground in a mortar. The mixture was introduced incrementally with mechanical stirring into a beaker containing 40 g of polyphosphoric acid (PPA) at 100 °C. Whitin a short period, the reaction mixture began releasing gaseous HCl. The temperature of the resulting viscous mixture was raised to 150 °C, and the mixture underwent a 12-hour reaction period while being continuously stirred. Subsequently, the mixture was transferred into 100 milliliters of cold water, and the pH of the resultant solution was adjusted to 5 by introducing a concentrated NaOH solution. A pale orange solid was obtained. Yield: 5.84 g (83%). M.p.: 277 °C. ^{1}H NMR (400 MHz, d6-DMSO) δ 5.94 (s, 2H), 6.04 (s, 2H), 7,50 (t, 1H), 8.91 (d, 1H).

Plate colorless crystals were obtained from slow evaporation of an ethanolic solution at room temperature in 24 h.

Triaz2: Commercial 2-picolinic acid (5.00, 40.6 mmol) and diaminoguanidine monohydrochloride (7.36 g, 58.6 mmol, 30% excess by mol) were finely ground in a mortar. The mixture was introduced incrementally with mechanical stirring into a beaker containing 40 g of polyphosphoric acid (PPA) at 100 °C. Whitin a short period, the reaction mixture began releasing gaseous HCl. The temperature of the resulting viscous mixture was raised to 150 °C, and the mixture underwent a 12-hour reaction period while being continuously stirred. Subsequently, the mixture was transferred into 100 milliliters of cold water, and the pH of the resultant solution was adjusted to 5 by introducing a concentrated NaOH solution. A pale-yellow solid was obtained. Yield 5.76 g

Preprints (www.preprints.org) | NOT PEER-REVIEWED | Posted: 2 November 2023 doi:10.20944/preprints202311.0186.v1

(80.5%). M.p.: 239 °C. ^{1}H NMR (400 MHz, d6-DMSO) δ 5.85 (s, 2H), 6.11 (s, 2H), 6.93 (m, 4H), 7.25 (t, 3H), 7.86 (d, 2H), 8.36 (d, 2H), 11.88(s, 1H).
Plate colorless crystals were obtained from slow evaporation of an ethanolic solution at room temperature in 24 h.

Triaz3-Triaz5: Diaminoguanidine monohydrochloride (5.00 g, 40 mmol, 15 % excess by mol) was finely ground in a mortar and mixed with 1.65 mL of formic acid (94% m/V, 34.5 mmol). The mixture was heated at reflux for 2h. The product was filtered under vacuum and washed with cold ethanol. 2.730 g of **DATr-HCl** in the form of a white solid were obtained (80 % Yield). ^{1}H NMR (400 MHz, d6-DMSO) δ 6.26 (s, 2H), 8.32 (s, 2H), 8.42 (s, 1H).

40 mg (0.3 mmol) of **DATr-HCl** were dissolved in 10 ml of hot water and 10 drops of HBr concentrated solution (48% v/v) were added. Prismatic colourless crystals of **Triaz3** were obtained by slow evaporation at room temperature in 2 days.

40 mg (0.3 mmol) of **DATr-HCl** were dissolved in 10mL of hot water together with 34 mg (0.15 mmol) of $ZnBr_2$ (again, 2:1 molar ratio) and 5 drops of concentrated hydrobromic acid (48% v/v). Prismatic colourless crystals of **Triaz4** were obtained in a week by slow evaporation of the solvent at Room Temperature.

40mg (0.3 mmol) of **DATr-HCl** were dissolved in 10 mL of hot water together with 21 mg (0.15 mmol) of $ZnCl_2$ (2:1 ratio by mol) and 5 drops of hydrochloric acid (37% v/v). The solution was left at room temperature for a week. The slow evaporation of the solvent led to the formation of prismatic colourless crystals of **Triaz5.**

3. Results and discussion

Crystal data of all studied triazoles are summarized in Table 1.

Table 1. Crystallographic information of the discussed compounds.

	Triaz1	Triaz2	Triaz3	Triaz4	Triaz5
Chemical Formula	$C_6H_7N_7$	$C_7H_9N_6{\cdot}H_2O_4P$	$C_2H_6N_5{\cdot}Br$	$2(C_2H_6N_5){\cdot}Br_4Zn$	$2(C_2H_6N_5){\cdot}Cl_4Zn$
M_r	177.19	274.19	180.03	585.25	407.41
Crystal system space group	Monoclinic, $P2_1/c$	Monoclinic, $C2/c$	Monoclinic, Cc	Monoclinic, Pc	Orthorhombic, $Pbca$
Temperature (K)	293	293	293	173	173
a, b, c (Å)	7.435 (3), 9.067 (3), 11.465 (4)	26.400 (7), 6.244 (3), 18.701 (6)	5.0140 (17), 15.288 (3), 7.937 (2)	7.539 (3), 12.059 (4), 11.144 (3)	16.9130 (17), 8.348 (4), 21.356 (8)
α, β, γ (°)	90, 106.98 (2), 90	90, 133.01 (2), 90	90, 99.33, 90	90, 129.48 (2), 90	90, 90, 90
V (Å^3)	739.2 (5)	2254.3 (15)	600.4 (3)	782.0 (5)	3015.2 (18)
Z	4	8	4	2	8
Radiation type	Mo $K\alpha$				
m (mm^{-1})	0.11	0.26	6.75	11.79	2.34
Crystal size (mm)	0.40 × 0.10 × 0.03	0.40 × 0.30 × 0.20	0.35 × 0.20 × 0.20	0.35 × 0.20 × 0.15	0.45 × 0.30 × 0.30
Diffractometer	Bruker-Nonius KappaCCD				
Absorption correction	Multi-scan *SADABS* (Bruker, 2001)				
T_{min}, T_{max}	0.940, 0.980	0.890, 0.936	0.190, 0.327	0.112, 0.259	0.410, 0.528
$I > 2\sigma(I)$]	4695, 1677, 1203	10432, 2582, 2015	1562, 1112, 1070	4720, 3082, 2918	11619, 3392, 2787
R_{int}	0.042	0.038	0.022	0.050	0.031
sin (θ/λ)$_{max}$ (Å^{-1})	0.650				

Preprints (www.preprints.org) | NOT PEER-REVIEWED | Posted: 2 November 2023 doi:10.20944/preprints202311.0186.v1

$R[F^2>2\sigma(F^2)]$, $wR(F^2)$, S	0.043, 0.110, 1.03	0.042, 0.102, 1.07	0.024, 0.061, 1.03	0.044, 0.119, 1.06	0.025, 0.054, 1.08
No. of reflections	1677	2582	1112	3082	3392
No. of parameters	130	184	92	168	202
No. of restraints	0	0	6	2	10
$\Delta\varrho_{max}$, $\Delta\varrho_{min}$ (e Å^{-3})	0.18, –0.24	0.27, –0.31	0.50, –0.49	1.27, –1.36	0.32, –0.38
Absolute structure			Flack x determined using 397 quotients [(I+)-(I-)]/ [(I+)+(I-)]	Refined as an inversion twin.	
Absolute structure parameter			0.065 (18)	0.05 (3)	

The X-ray molecular structure of **Triaz1** is shown in Figure 1.

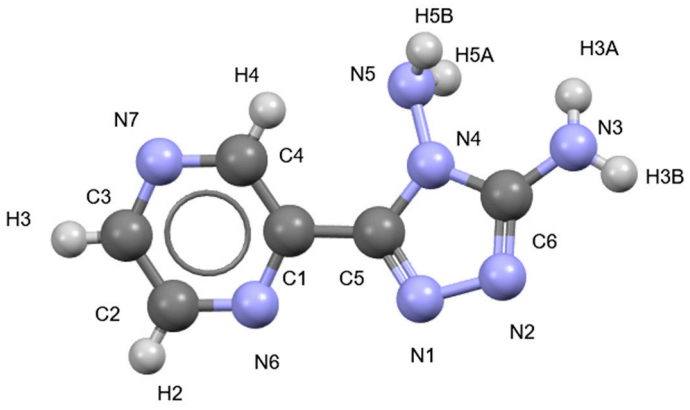

Figure 1. The X-ray molecular structure of **Triaz1.**

Both amino N atoms have a pyramidal geometry. In the case of CNH_2 the pyramidal geometry is more flat (sum of valence angles at N3 is 350(5)°) than for NNH_2 (sum of valence angles at N5 is 327(4)°). This is indicative of a partial π-conjugation of CNH_2 amino group with the aromatic system of the triazole ring.

The molecular conformation of **Triaz1** is determined by the little twist around the C1-C5 bond, which produces a dihedral angle of 19.32(2)° between the average planes of the pyrazinyl and triazole moieties. The twist could be accounted for the formation of suitable angles for H-bond interactions of both N6 and N7 acceptor atoms. In fact, as shown in Figure 2a, the pyrazyl ring is involved in two strong hydrogen bond interactions between two layers of **Triaz1** with a distance of 2.438(3) and 2.269(2) Å.

Preprints (www.preprints.org) | NOT PEER-REVIEWED | Posted: 2 November 2023 doi:10.20944/preprints202311.0186.v1

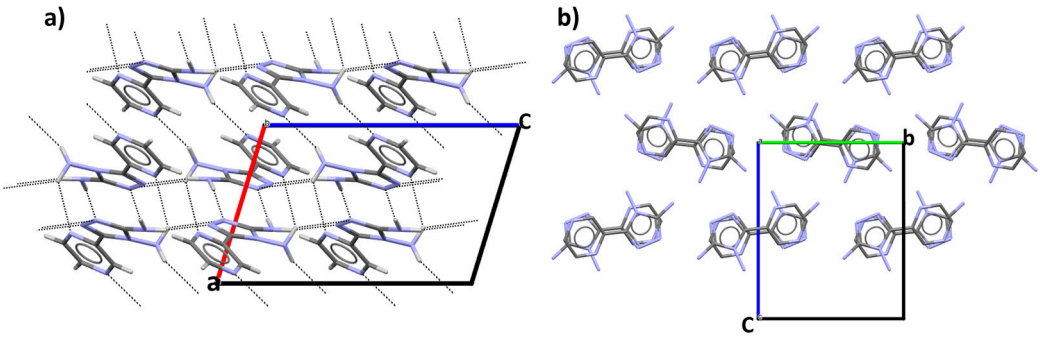

Figure 2. Triaz1 crystal packing: (**a**) view along *b* axis; (**b**) view along *a* axis. Hydrogen bond interaction in dashed lines.

Diamminotriazole molecules in the layer are held by a strong homomeric NCNH2 $R_2^2(8)$ motif, [35–37] with a distance of 2.305(2) Å. The 2_1 axis and the *c* glide plane build alternate layers of diaminotriazole molecules with a stacking distance of 3.288(5) (Figure 2b). For a more in-depth examination of intermolecular interactions, we utilized the CrystalExplorer 21.5 program to calculate two-dimensional (2D) fingerprints and the corresponding Hirshfeld Surfaces (HS) for all the compounds. As depicted in Figure 3, the red areas on the HS signify close contacts in the shape of intermolecular hydrogen bonds, encompassing N···H and H···N interactions, which contribute to 46% of the crystal packing and confirm the significant role of homomeric synthons in the structure. The directional C···H close contacts are associated with π···H interaction of the aromatic rings with the surrounding molecules and contribute in all the five compounds for less of the 10%. The high value of H···H close contacts in this crystal structure could be associated to a close distance of the molecules in the crystal packing.

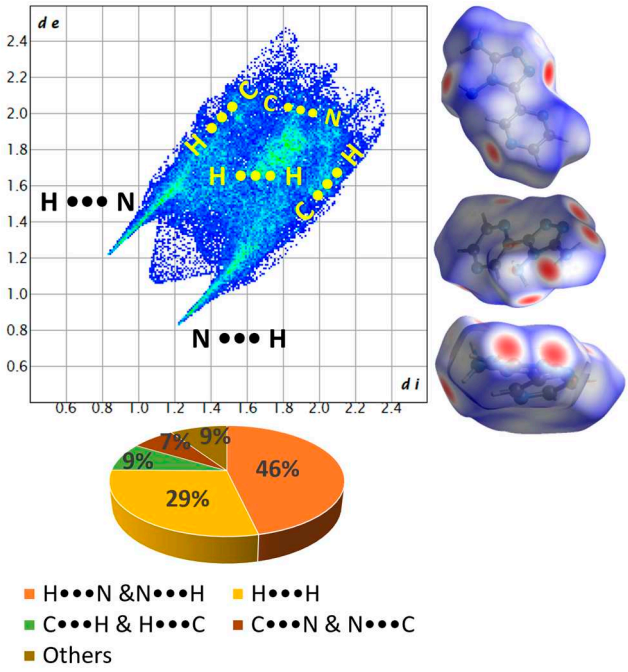

Figure 3. Hirshfeld fingerprint plot of the **Triaz1** compound with potential energy surface.

The X-ray molecular structure of **Triaz2** is shown in Figure 4.

Preprints (www.preprints.org) | NOT PEER-REVIEWED | Posted: 2 November 2023 doi:10.20944/preprints202311.0186.v1

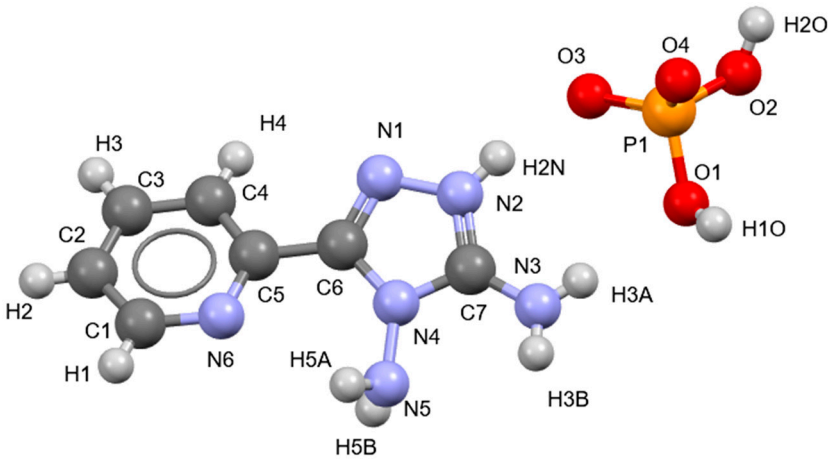

Figure 4. The crystal structure of **Triaz2.**

Protonation of the triazole is at the N ring atom adjacent to CNH_2 carbon, i. e. at N2. This feature, that holds unchanged for all singly protonated triazoles reported in this paper (*vide ultra*), is related with the stabilization of the positive charge on N2 by the electron donor NH_2 group on the adjacent carbon atom. As a result of this stabilization, the geometry around CNH_2 amino nitrogen is planar trigonal (sum of valence angles at N3 is 358(7)°). On the other hand, the geometry around NNH_2 amino nitrogen is pyramidal as in the neutral triazole (sum of valence angles at N5 is 326(7)°).

The conformation of **Triaz2,** as for **Triaz1**, is characterized by a little twist of the pyridine ring with respect to the triazole ring with the formation of a dihedral angle of 18.82(4)°. Differently from **Triaz1**, in this case the twist can be related to the ability of the triazole amino group close to the N6 to establish strong H-bond interaction with the O2 atom of the dihydrogen phosphate counter ion (Figure 5b). The cationic diaminotriazole molecules interact with the inorganic contour anion by establishing a strong heteromeric NH2NCH POO $R_2^2(8)$ ring pattern, with distance values of 1.861(3), 2.014(3) and 2.171(3) Å (Figure 5a) [38–40]. Molecules in the crystal are arranged in a stair motif in which each diaminotriazole layer is linked to the other through the interaction with the counterion (Figure 5b). The tautomer isolated for this compound has H atom bonded to N2 rather than N6, which is sterically hindered for this molecular conformation.

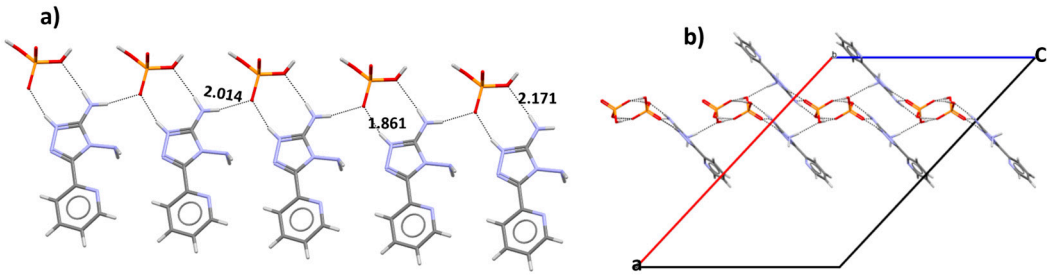

Figure 5. Triaz2 crystal packing: (**a**) Hydrogen bond interaction along the *b* axis; (**b**) view along the *b* axis. Hydrogen bond interaction in dashed lines.

The HS surface analysis, Figure 6, confirms that the packing is strongly influenced by the hydrogen bond interaction between the charged molecules while differently from **Triaz1** the N···H and H···N interactions are less relevant. For **Triaz2** it is calculated the highest value of H···H close contacts in the set of crystal structures studied in this paper.

Preprints (www.preprints.org) | NOT PEER-REVIEWED | Posted: 2 November 2023 doi:10.20944/preprints202311.0186.v1

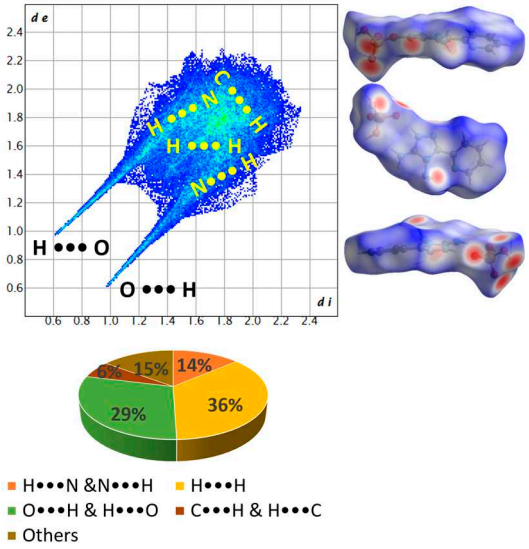

Figure 6. Hirshfeld fingerprint plot of **Triaz2** with potential energy surface.

In Figure 7 are reported the crystal structures of **Triaz3, Triaz4** and **Triaz5.**

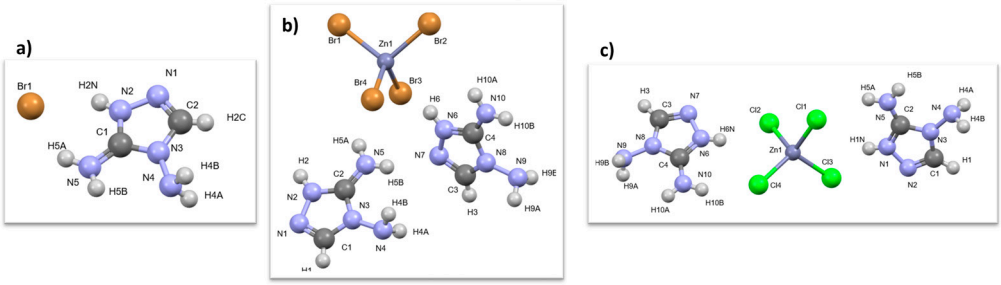

Figure 7. The crystal structures of a) **Triaz3,** b) **Triaz4**, c) **Triaz5.**

All three crystalline structures share the same diamminotriazole cation (**DATr**) but with three different counterions, bromide ion (Figure 7a), tretrachlobromide (Figure 7b) and tetrachlorozincate (Figure 7b) respectively. As previously stated, in all triazole cations protonation is on the N ring atom adjacent to CNH_2 carbon. As a result, amino CNH_2 atom is planar trigonal (sum of valence angles at N is always 360°) , while NNH_2 keeps the pyramidal geometry, as in the neutral triazole **Triaz1** and protonated triazole of **Triaz2**.

The crystal packings are strongly influenced by hydrogen bond interactions between **DATr** cation and the halogen of the counter ion (Figure 8) with distances and angles reported in Table 3 confirmed by the HS fingerplot that highlights a high contribute of these interactions with a maximum of 49% for **Triaz4** (Figure 8 center). On the other hand, **Triaz3** and **Triaz5** show a major contribute of N···H interaction with a 25% and 22% respectively.

The crystal packings of **Triaz3, Triaz4** and **Triaz5** show scaffold of inorganic counter anions spaced out by scaffold of organic cations (Figure 9).

Table 2. Hydrogen bond geometry of **Triaz3**, **Triaz4**, **Triaz5**.

	D—H···*A*	H···*A* (Å)	*D*—H···*A* (°)
Triaz3	N2—H2N···Br1	2.47(8)	155(7)
	N4—H4A···Br1	2.75(4)	147(6)
	N4—H4B···Br1	2.63(4)	157(5)
	N5—H5A···Br1	2.84(5)	138(6)
	N5—H5A···Br1	2.91(6)	123(6)
	N5—H5B···N1	2.12(4)	159(7)

Preprints (www.preprints.org) | NOT PEER-REVIEWED | Posted: 2 November 2023 doi:10.20944/preprints202311.0186.v1

Triaz4	C1—H1···Br1	2.65	166.6
	N2—H2···N4	2.18	165.5
	N4—H4A···Br2	2.65	166.0
	N4—H4B···Br1	2.44	162.8
	N5—H5A···Br4	2.68	145.9
	N5—H5B···N7	2.18	162.8
	N9—H9B···Br4	2.94	157.6
	N10—H10A···Br4	2.80	165.8
	N10—H10B···Br3	2.73	166.3
	N6—H6···N1	2.06	150.6
Triaz5	N1—H1N···Cl1	2.775(19)	132.5(18)
	N1—H1N···Cl3	2.584(18)	143.2(19)
	N4—H4A···Cl2	2.880(18)	142.8(18)
	N4—H4B···Cl3	2.782(19)	135.4(18)
	N5—H5A···Cl1	2.507(18)	149(2)
	N5—H5B···N7	2.113(16)	167(2)
	N6—H6N···Cl2	2.370(18)	150(2)
	N9—H9B···Cl3	2.654(18)	141.818)
	N10—H10A···Cl3	2.404(17)	176(2)
	N10—H10B···N2	2.63(3)	113(2)
	N10—H10B···Cl4	2.586(18)	158(2)

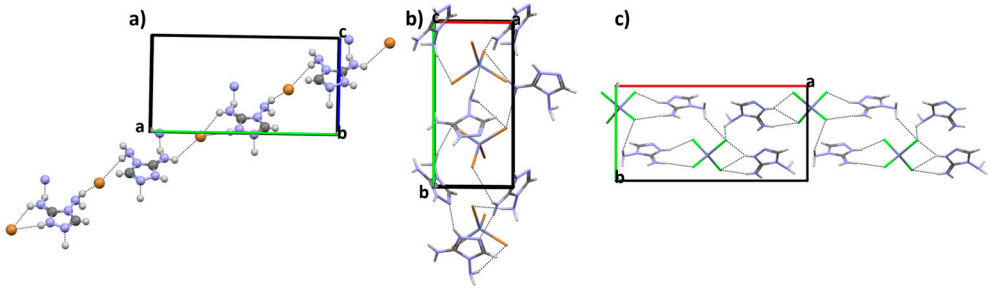

Figure 8. Hydrogen bonding patterns: a) **Triaz3 b**) **Triaz4** c) **Triaz5.** Hydrogen bond interactions in dashed lines.

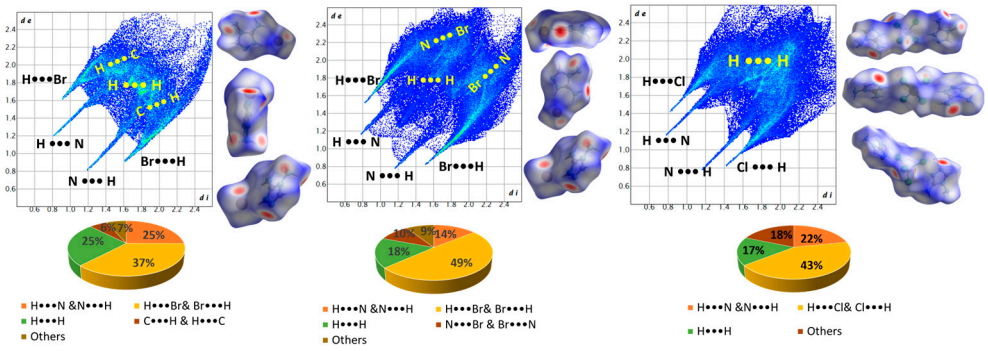

Figure 9. Hirshfeld fingerprint plot of **Triaz3** (left), **Triaz4** (center) and **Triaz5** (right) with potential energy surface.

Preprints (www.preprints.org) | NOT PEER-REVIEWED | Posted: 2 November 2023 doi:10.20944/preprints202311.0186.v1

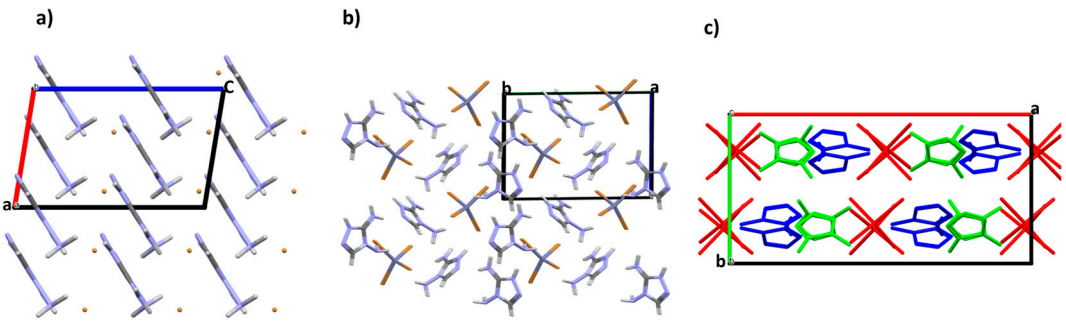

Figure 10. Crystal packing of a) **Triaz3** along *b* axis **b**) **Triaz4** along *c* axis and c) **Triaz5** along *a* axis.

4. Conclusions

In conclusion, a novel series of N-Rich triazole derivatives by using the diaminoguanidine hydrochloride, as building block compound, were synthesized and crystallized. Utilizing NMR spectroscopy and single X-ray diffraction measurements, the structures of synthesized compounds were verified and determined. The supramolecular features of the compounds were analyzed with Hirshfeld topology that highlight an high presence of strong H-bond driven by the amino group of the diaminotriazole moieties. **Triaz1** crystal packing is strongly driven by the homomeric NCNH2 $R_2^2(8)$ supramolecular synthon with a very high contribute (46%). Similarly**, Triaz2** crystal packing is influenced by the presence of the heteromeric NH2NCH POO $R_2^2(8)$ ring pattern with a contribute of 29%. The crystal packings of **Triaz3**,**Triaz4**, and **Triaz5** highlight a strong presence of strong H-bond interactions between the donor amino group of the triazole block with the halogen acceptor atoms of the counterions. These new systems, thanks to a high nitrogen content in the molecular backbone, could open to a new series of materials potentially relevant for applications affecting the industry of high energy density materials, as an application in the field of explosives or propellant gases with low toxicity.

Supplementary Materials: The following supporting information can be downloaded at: NMR spectra of **Triaz1**, **Triaz2**, **DATr-HCl.** CCDC number of the deposited Crystal structure: 2304297, 2304298, 2304299, 2304303, 2304304.

Author Contributions: The manuscript was written through contributions of both the authors, and both the authors have given approval to the final version of the manuscript.

Conflict of Interest: The authors declare no conflict of interest.

References

1. Martins, P.; Jesus, J.; Santos, S.; Raposo, L.R.; Roma-Rodrigues, C.; Baptista, P.V.; Fernandes, A.R. Heterocyclic Anticancer Compounds: Recent Advances and the Paradigm Shift towards the Use of Nanomedicine's Tool Box. *Molecules* **2015**, *20*, 16852–16891, doi:10.3390/molecules200916852.
2. Heeger, A.J. Semiconducting Polymers: The Third Generation. *Chem Soc Rev* **2010**, *39*, 2354–2371, doi:10.1039/b914956m.
3. Miao, Q. Ten Years of N-Heteropentacenes as Semiconductors for Organic Thin-Film Transistors. *Advanced Materials* **2014**, *26*, 5541–5549, doi:10.1002/adma.201305497.
4. Argeri, M.; Borbone, F.; Caruso, U.; Causà, M.; Fusco, S.; Panunzi, B.; Roviello, A.; Shikler, R.; Tuzi, A. Color Tuning and Noteworthy Photoluminescence Quantum Yields in Crystalline Mono-/Dinuclear ZnII Complexes. *Eur J Inorg Chem* **2014**, *2014*, 5916–5924, doi:10.1002/ejic.201402717.
5. Fusco, S.; Parisi, E.; Volino, S.; Manfredi, C.; Centore, R. Redox and Emission Properties of Triazolo-Triazole Derivatives and Copper(II) Complexes. *J Solution Chem* **2020**, *49*, 504–521, doi:10.1007/s10953-020-00975-3.
6. Maglione, C.; Carella, A.; Centore, R.; Chávez, P.; Lévêque, P.; Fall, S.; Leclerc, N. Novel Low Bandgap Phenothiazine Functionalized DPP Derivatives Prepared by Direct Heteroarylation:

Application in Bulk Heterojunction Organic Solar Cells. *Dyes and Pigments* **2017**, *141*, 169–178, doi:10.1016/j.dyepig.2017.02.012.

7. B. Nielsen, C.; Holliday, S.; Chen, H.-Y.; J. Cryer, S.; McCulloch, I. Non-Fullerene Electron Acceptors for Use in Organic Solar Cells. *Acc Chem Res* **2015**, *48*, 2803–2812, doi:10.1021/acs.accounts.5b00199.
8. Klapötke, T.M. *Chemistry of High-Energy Materials*; 5th ed.; de Gruyter, 2019;
9. Klapötke, T.M.; Schmid, Philipp.C.; Schnell, S.; Stierstorfer, J. Thermal Stabilization of Energetic Materials by the Aromatic Nitrogen-Rich 4{,}4′{,}5{,}5′-Tetraamino-3{,}3′-Bi-1{,}2{,}4-Triazolium Cation. *J. Mater. Chem. A* **2015**, *3*, 2658–2668, doi:10.1039/C4TA05964F.
10. Parisi, E.; Landi, A.; Fusco, S.; Manfredi, C.; Peluso, A.; Wahler, S.; M. Klapötke, T.; Centore, R. High-Energy-Density Materials: An Amphoteric N-Rich Bis(Triazole) and Salts of Its Cationic and Anionic Species. *Inorg Chem* **2021**, *0*, doi:10.1021/acs.inorgchem.1c02002.
11. Hu, L.; Staples, R.J.; Shreeve, J.M. Energetic Compounds Based on a New Fused Triazolo [4,5-d]Pyridazine Ring: Nitroimino Lights up Energetic Performance. *Chemical Engineering Journal* **2021**, *420*, 129839, doi:https://doi.org/10.1016/j.cej.2021.129839.
12. Fusco, S.; Parisi, E.; Carella, A.; Capobianco, A.; Peluso, A.; Manfredi, C.; Borbone, F.; Centore, R. Solid State Selection between Nearly Isoenergetic Tautomeric Forms Driven by Right Hydrogen-Bonding Pairing. *Cryst Growth Des* **2018**, *18*, 6293–6301, doi:10.1021/acs.cgd.8b01158.
13. Fusco, S.; Parisi, E.; Volino, S.; Manfredi, C.; Centore, R. Redox and Emission Properties of Triazolo-Triazole Derivatives and Copper(II) Complexes. *J Solution Chem* **2020**, *49*, 504–521, doi:10.1007/s10953-020-00975-3.
14. Pagacz-Kostrzewa, M.; Bil, A.; Wierzejewska, M. UV-Induced Proton Transfer in 3-Amino-1,2,4-Triazole. *J Photochem Photobiol A Chem* **2017**, *335*, 124–129, doi:10.1016/j.jphotochem.2016.11.023.
15. Parisi, E.; Capasso, D.; Capobianco, A.; Peluso, A.; Di Gaetano, S.; Fusco, S.; Manfredi, C.; Mozzillo, R.; Pinto, G.; Centore, R. Tautomeric and Conformational Switching in a New Versatile N-Rich Heterocyclic Ligand. *Dalton Transactions* **2020**, *49*, 14452–14462, doi:10.1039/d0dt02572k.
16. Parisi, E.; Centore, R. Stabilization of an Elusive Tautomer by Metal Coordination. *Acta Crystallographica Section C* **2021**, *77*, 395–401, doi:10.1107/S2053229621006203.
17. Capobianco, A.; Di Donato, M.; Caruso, T.; Centore, R.; Lapini, A.; Manfredi, C.; Velardo, A.; Volino, S.; Peluso, A. Phototautomerism of Triazolo-Triazole Scaffold. *J Mol Struct* **2020**, *1203*, doi:10.1016/j.molstruc.2019.127368.
18. Sutradhar, M.; Alegria, E.C.B.A.; Mahmudov, K.T.; Guedes Da Silva, M.F.C.; Pombeiro, A.J.L. Iron(III) and Cobalt(III) Complexes with Both Tautomeric (Keto and Enol) Forms of Aroylhydrazone Ligands: Catalysts for the Microwave Assisted Oxidation of Alcohols. *RSC Adv* **2016**, *6*, 8079–8088, doi:10.1039/c5ra25774c.
19. Parisi, E.; Carella, A.; Borbone, F.; Chiarella, F.; Gentile, F.S.; Centore, R. Effect of Chalcogen Bonding on the Packing and Coordination Geometry in Hybrid Organic–Inorganic Cu(Ii) Networks. *CrystEngComm* **2022**, *24*, 2884–2890, doi:10.1039/D2CE00069E.
20. Gentile, F.S.; Parisi, E.; Centore, R. Journeys in Crystal Energy Landscapes: Actual and Virtual Structures in Polymorphic 5-Nitrobenzo [c] [1,2,5]Thiadiazole. *CrystEngComm* **2023**, *25*, 859–865, doi:10.1039/D2CE01619B.
21. Centore, R.; Borbone, F.; Carella, A.; Causà, M.; Fusco, S.; Gentile, F.S.; Parisi, E. Hierarchy of Intermolecular Interactions and Selective Topochemical Reactivity in Different Polymorphs of Fused-Ring Heteroaromatics. *Cryst Growth Des* **2020**, *20*, 1229–1236, doi:10.1021/acs.cgd.9b01491.
22. Fusco, S.; Capasso, D.; Centore, R.; Di Gaetano, S.; Parisi, E. A New Biologically Active Molecular Scaffold: Crystal Structure of 7-(3-Hydroxyphenyl)-4-Methyl-2H- [1,2,4]Triazolo [3,2-c] [1,2,4]Triazole and Selective Antiproliferative Activity of Three Isomeric Triazolo-Triazoles. *Acta Crystallogr C Struct Chem* **2019**, *75*, 1398–1404, doi:10.1107/S2053229619012403.
23. Centore, R.; Carella, A.; Fusco, S. Supramolecular Synthons in Fluorinated and Nitrogen-Rich Ortho-Diaminotriazoles. *Struct Chem* **2011**, *22*, 1095–1103, doi:10.1007/s11224-011-9805-0.

24. Centore, R.; Fusco, S.; Capobianco, A.; Piccialli, V.; Zaccaria, S.; Peluso, A. Tautomerism in the Fused N-Rich Triazolotriazole Heterocyclic System. *European J Org Chem* **2013**, 3721–3728, doi:10.1002/ejoc.201201653.
25. Li, Z.; Zhang, J.; Cui, Y.; Zhang, T.; Shu, Y.; Sinditskii, V.P.; Serushkin, V. V; Egorshin, V.Yu. A Novel Nitrogen-Rich Cadmium Coordination Compound Based on 1,5-Diaminotetrazole: Synthesis, Structure Investigation, and Thermal Properties. *J Chem Eng Data* **2010**, *55*, 3109–3116.
26. Emilsson, K.; Selander, L.H. Bho. *European Journal Medicinal Chemistry* **1986**, *21*, 235.
27. Trust, R.I.; Albright, J.D.; Lovell, F.M.; Perkinson, N.A. 6- and 7-Aryl-1,2,4-Triazolo [4,3-b]-1,2,4-Triazines. Synthesis and Characterization. *J Heterocycl Chem* **1979**, *16*, 1393–1403, doi:https://doi.org/10.1002/jhet.5570160721.
28. Bruker-Nonius (2002) . SADABS, Bruker-Nonius, Delft, The Netherlands.
29. Altomare, A.; Burla, M.C.; Camalli, M.; Cascarano, G.L.; Giacovazzo, C.; Guagliardi, A.; Moliterni, A.G.G.; Polidori, G.; Spagna, R. SIR97: A New Tool for Crystal Structure Determination and Refinement. *J Appl Crystallogr* **1999**, *32*, 115–119, doi:10.1107/S0021889898007717.
30. Sheldrick, G.M. Crystal Structure Refinement with SHELXL. *Acta Crystallogr C Struct Chem* **2015**, *71*, 3–8, doi:10.1107/S2053229614024218.
31. Farrugia, L.J. WinGX and ORTEP for Windows: An Update. *J Appl Crystallogr* **2012**, *45*, 849–854, doi:10.1107/S0021889812029111.
32. Macrae, C.F.; Bruno, I.J.; Chisholm, J.A.; Edgington, P.R.; McCabe, P.; Pidcock, E.; Rodriguez-Monge, L.; Taylor, R.; Van De Streek, J.; Wood, P.A. Mercury CSD 2.0 - New Features for the Visualization and Investigation of Crystal Structures. *J Appl Crystallogr* **2008**, *41*, 466–470, doi:10.1107/S0021889807067908.
33. Spackman, M.A.; Jayatilaka, D. Hirshfeld Surface Analysis. *CrystEngComm* **2009**, *11*, 19–32, doi:10.1039/B818330A.
34. Lieber, Eugene.; B. L. Smith, G. The Chemistry of Aminoguanidine and Related Substances. *Chem Rev* **2002**, *25*, 213–271, doi:10.1021/cr60081a003.
35. Kennedy, A.R.; Khalaf, A.I.; Suckling, C.J.; Waigh, R.D. Methyl 2-Amino-5-Isopropyl-1,3-Thiazole-4-Carboxylate. *Acta Crystallographica Section E* **2004**, *60*, o1510–o1512, doi:10.1107/S1600536804019282.
36. Stierstorfer, J.; Tarantik, K.R.; Klapötke, T.M. New Energetic Materials: Functionalized 1-Ethyl-5-Aminotetrazoles and 1-Ethyl-5-Nitriminotetrazoles. *Chemistry – A European Journal* **2009**, *15*, 5775–5792, doi:https://doi.org/10.1002/chem.200802203.
37. Wang, C.; Hu, S.; Sun, C.C. Expedited Development of a High Dose Orally Disintegrating Metformin Tablet Enabled by Sweet Salt Formation with Acesulfame. *Int J Pharm* **2017**, *532*, 435–443, doi:https://doi.org/10.1016/j.ijpharm.2017.08.100.
38. Kaynak, F.B.; Eriksson, L.; Salgın-Gökşen, U.; Gökhan-Kelekçi, N. Molecular Structure of 2-Methylamino-5- [(5-Methyl-2-Benzoxazolinone-3-Yl)Methyl]-1,3,4-Thiadiazole Dihydrophosphate: A Combined X-Ray Crystallographic and Ab Initio Study. *Struct Chem* **2008**, *19*, 757–764, doi:10.1007/s11224-008-9360-5.
39. Matulková, I.; Fábry, J.; Eigner, V.; Dušek, M.; Kroupa, J.; Němec, I. Isostructural Crystals of Bis(Guanidinium) Trioxofluoro-Phosphate/Phosphite in the Ratio 1/0, 0.716/0.284, 0.501/0.499, 0.268/0.732, 0/1—Crystal Structures, Vibrational Spectra and Second Harmonic Generation. *Crystals (Basel)* **2022**, *12*, doi:10.3390/cryst12121694.
40. Radanović, M.M.; Rodić, M. V; Armaković, S.; Armaković, S.J.; Vojinović-Ješić, L.S.; Leovac, V.M. Pyridoxylidene Aminoguanidine and Its Copper(II) Complexes – Syntheses, Structure, and DFT Calculations. *J Coord Chem* **2017**, *70*, 2870–2887, doi:10.1080/00958972.2017.1367388.